Tunable Lattice Reconstruction, Triangular Network of Chiral One-Dimensional States, and Bandwidth of Flat Bands in Magic Angle Twisted Bilayer Graphene

Yi-Wen Liu,[1,†] Ying Su,[2,†] Xiao-Feng Zhou,[1] Long-Jing Yin,[1,3] Chao Yan,[1] Si-Yu Li,[1,4] Wei Yan,[1] Sheng Han,[1] Zhong-Qiu Fu,[1] Yu Zhang,[1] Qian Yang,[1] Ya-Ning Ren,[1] and Lin He[1,*]

[1]*Center for Advanced Quantum Studies, Department of Physics, Beijing Normal University, Beijing 100875, People's Republic of China*

[2]*Theoretical Division, T-4 and CNLS, Los Alamos National Laboratory, Los Alamos, New Mexico 87545, USA*

[3]*Key Laboratory for Micro/Nano Optoelectronic Devices of Ministry of Education and Hunan Provincial Key Laboratory of Low-Dimensional Structural Physics and Devices, School of Physics and Electronics, Hunan University, Changsha 410082, China*

[4]*Key Laboratory for Micro-Nano Physics and Technology of Hunan Province, College of Materials Science and Engineering, Hunan University, Changsha 410082, People's Republic of China*

(Received 26 July 2020; accepted 2 November 2020; published 1 December 2020)

The interplay between interlayer van der Waals interaction and intralayer lattice distortion can lead to structural reconstruction in slightly twisted bilayer graphene (TBG) with the twist angle being smaller than a characteristic angle θ_c. Experimentally, the θ_c is demonstrated to be very close to the magic angle ($\theta \approx 1.08°$). Here we address the transition between reconstructed and unreconstructed structures of the TBG across the magic angle by using scanning tunneling microscopy (STM). Our experiment demonstrates that both structures are stable in the TBG around the magic angle. By using a STM tip, we show that the two structures can be changed to each other and a triangular network of chiral one-dimensional states hosted by domain boundaries can be switched on and off. Consequently, the bandwidth of the flat band, which plays a vital role in the emergent strongly correlated states in the magic angle TBG, is tuned. This provides an extra control knob to manipulate the exotic electronic states of the TBG near the magic angle.

DOI: 10.1103/PhysRevLett.125.236102

Twisted bilayer graphene (TBG) formed by a vertical stacking of two misaligned graphene layers has increasingly attracted considerable interest [1–7]. Remarkably, at the so-called magic angle ($\theta \approx 1.08°$), the low-energy bands around the charge neutrality become nearly flat. The quench of the kinetic energy of quasiparticles, which is determined by the electronic bandwidth of the flat bands, results in many strongly correlated states in TBG [8–13]. Very recently, it was demonstrated that there is structural reconstruction in slightly TBG because of the competition between the interlayer van der Waals coupling and the intralayer elastic deformation [14–21]. Experimentally [19], structural reconstruction occurs in the TBG with twist angle $\theta \leq \theta_c \sim 1°$. Obviously, the characteristic crossover angle θ_c between the reconstructed and unreconstructed structures is very close to the magic angle.

In this Letter, we systematically studied the structures of TBG around the magic angle by using scanning tunneling microscopy (STM) and demonstrated that both the reconstructed and unreconstructed structures can be stable around the magic angle. By applying a STM tip pulse, the two structures can be changed to each other, and a triangular network of chiral one-dimensional states hosted by domain boundaries can be switched on and off. Consequently, the bandwidth of the flat bands is also changed dramatically. Our result not only offers a reasonable explanation to understand the quite different electronic properties observed in the magic angle TBG (MATBG), but also provides a new route to manipulate the exotic electronic phases.

In our experiments, large aligned monolayer graphene was synthesized on Cu foil [22–25] (see Supplemental Figs. S1 and S2 for details of the growth [26]). Then, through a conventional wet etching technique, the monolayer graphene was transferred layer by layer onto different target substrates, involving 0.7% Nb-doped $SrTiO_3$ (001), a Si/SiO_2 wafer, Ag-coated mica, and Cu (111) substrates, to obtain the TBG with a controlled twist angle (see Fig. S3 for details of the fabrication and Fig. S4 for STM characterizations of the substrates and the obtained TBG [26]). Despite the angle-dependent electronic properties of the TBG having been extensively studied in STM studies, the angle-dependent lattice reconstruction is rarely explored. Figures 1(a)–1(d) show representative STM images of the obtained TBG with four different twist angles. The moiré superlattice can be clearly identified from the periodic corrugations at the AA stacking regions. For the TBG with $\theta = 17.76°$, the variation of height between h_{AA} at the AA regions and h_{AB} (h_{BA}) at the AB (BA) regions is only about 2 pm, as shown in Fig. 1(e). However, it increases to about

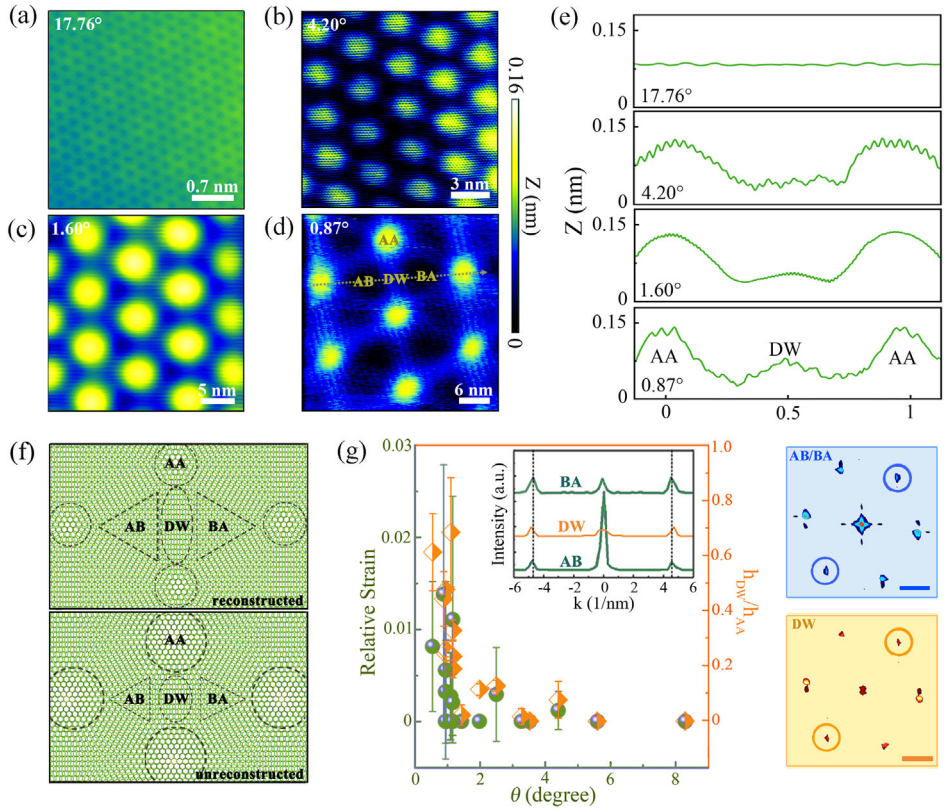

FIG. 1. (a)–(d) Typical STM images of four different TBGs ($V_S = 400$ mV, $I = 0.2$ nA). The *AA*, *AB*, *BA*, and DW regions are marked in (d). (e) Height profiles recorded at TBG along the yellow arrow, as shown in (d). The x axis is normalized by the spacing between two *AA* regions. (f) Schematic reconstructed and unreconstructed structures of TBG. (g) Left panel: Relative strain and the height ratio of different TBGs. The relative strain is calculated according to the ratio between the lattice constant in the DW region and that in the *AB* or *BA* region. The average lattice constant is obtained according to the FFT. Right panel: Representative FFT of the DW and *AB* and *BA* regions. The six bright spots are reciprocal lattices of graphene. Scale bar: 2.5 nm^{-1}. Inset: Section views cross the colored circles in the FFT. The dashed lines label the peaks obtained in the *AB* and *BA* regions.

60 pm for the TBG with $\theta \leq 4.2°$. The less lattice corrugation at a larger twist angle is due to the fact that the interlayer coupling in TBG falls off rapidly with an increasing twist angle [4,7]. For the TBG with $\theta = 0.87°$, as shown in Fig. 1(d), we can observe a clear signature of lattice reconstruction in the TBG: The *AA* regions are reduced, while the *AB* and *BA* regions are enlarged to minimize the global energy of the system [14–21]. In the meantime, the domain walls (DWs) separating adjacent *AB* and *BA* regions are corrugated [see Fig. 1(e); the height of the DWs is labeled as h_{DW}] and form a triangular network connecting different *AA* regions. The rearrangement of atomic registries in reconstructed and unreconstructed TBG is schematically shown in Fig. 1(f). For the reconstructed small angle TBG, it prefers to change the position of the lattice sites through losing elastic energy and gaining van der Waals energy [27], and then the nearly commensurate structure which is close to *AB* and *BA* structures separated by a narrow DW expand after the reconstruction. In contrast, when the van der Waals energy cannot compensate for the elastic energy at a large twist angle, it can be seen as two "independent" and "rigid" graphene layers without any lattice rearrangement, i.e., unreconstruction. According to a recent transmission electron microscopy study [19], the transition from structural unreconstruction to reconstruction occurs in TBG at the characteristic crossover angle $\theta_c \sim 1°$. In our STM measurements, we can obtain the evolution of structural reconstruction with the twist angle in two different ways, as summarized in Fig. 1(g). The first one is based on the relative strain between the DW and *AB* and *BA* regions as a function of the twist angle. Here the relative strain is estimated from the fast Fourier transformation (FFT) of different regions in the STM images, as shown in Fig. 1(g) (see Supplemental Fig. S5 for more details [26]), and the measured strain increases quite quickly with decreasing the twist angle below the characteristic crossover angle. The second method is based on the height ratio between the DW and *AA* regions h_{DW}/h_{AA} as a function of the twist angle [Fig. 1(g)], which shows a similar behavior as the relative strain vs the twist angle. Obviously, the characteristic crossover angle for structural reconstruction in TBG is around the magic angle.

One of the most prominent features in the reconstructed TBG is the emergence of *AB*-*BA* DWs that form a

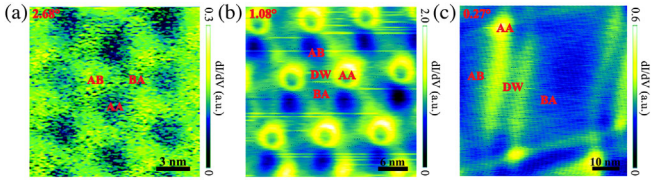

FIG. 2. (a)–(c) dI/dV maps of three TBGs. The experimental parameters are (a) $Vs = -35$ mV; (b) $V_S = 20$ mV; and (c) $V_S = 40$ mV. The different stacking regions are marked in the maps.

triangular network connecting different *AA* regions. In this case, the *AB* and *BA* regions are gapped and have opposite valley Chern numbers that guarantee the appearance of topological helical edge states at the DWs [28–41]. Such a feature can be directly imaged by carrying out the energy-fixed scanning tunneling spectroscope (STS) mapping [34,40,41], which reflects the local density of states (LDOS) in real space [40–48]. Figure 2 shows three representative STS maps of three different TBGs. For the TBG with $\theta = 2.68°$, the distribution of the LDOS exhibits the same period and symmetry of the moiré pattern in the STM image (see Supplemental Fig. S6 for the STM image and STS spectra [26]), and no signal of the DW can be observed [Fig. 2(a)]. As the twist angle decreases to the magic angle $\theta = 1.08°$, the triangular network of the *AB*-*BA* DWs connecting the *AA* regions appears, as shown in Fig. 2(b). Additionally, bright halos around the dark *AA* regions, as observed in previous studies [40,49], are also observed in the 1.08º TBG. With further lowering the twist angle to $\theta = 0.27°$, the conspicuous topological channels linking different *AA* stacking regions can be more clearly identified in Fig. 2(c). The width of the DW is as large as 10 nm, which allows us to observe the characteristic feature that the topological states are mainly located at the two edges of the DW, as observed previously in wide *AB*-*BA* DWs [34,40,41]. The missing domain wall mode that connects *AA* to *AA* sites diagonally arises from the heterostrain that leads to a tetragonal structural transition in the moiré pattern of tiny-angle TBG [41]. Obviously, it is convenient to know the structure of the TBG according to whether there is or not the triangular network of domain walls in the STM measurements.

In TBG, structural reconstruction arises from the competition between the interlayer van der Waals coupling and the intralayer elastic deformation [14–21]. For TBG with the twist angle below the magic angle, the size of the moiré pattern is quite large. Therefore, the *AB* and *BA* stacking regions prefer to be enlarged to reduce the cost of stacking energy, and, consequently, the TBG is reconstructed. For TBG with the twist angle that is much larger than the magic angle, the size of the moiré pattern is quite small. Hence, the rigid TBG structure can minimize the intralayer elastic energy and is energetically preferable. Therefore, for TBG around the magic angle, i.e., in the crossover region, the

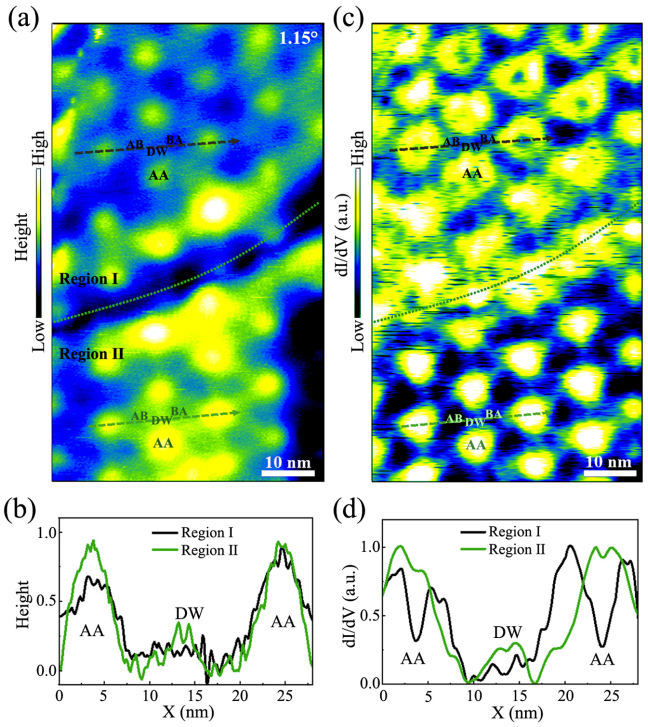

FIG. 3. (a) STM image of a TBG showing both the unreconstructed (region I) and reconstructed structures (region II) ($V_S = 30$ mV, $I = 0.4$ nA), which are separated by a dashed line. (b) Height profiles along dashed arrows in (a). (c) Typical dI/dV map of TBG at the energy of 30 meV. (d) dI/dV profiles along dashed arrows in (c).

global energy for the reconstructed and unreconstructed structures should be comparable. However, direct observation of the two structures in TBG at the crossover angle is still lacking up to now. In our experiment, we directly observed both the reconstructed and unreconstructed structures in TBG around the magic angle. Figures 3(a)–3(d) summarize STM measurements on TBG with $\theta = 1.15°$. Both the STM image and STS map of the 1.15º TGB show the coexistence of the two structures that are separated by a boundary, as marked by the dashed line in Figs. 3(a) and 3(c). Here we denote the area above (below) the boundary as region I (II). Even though the period of the moiré pattern (or the twist angle) in the two regions is the same, much clearer triangular networks of topological edge states along the *AB*-*BA* DWs are observed in region II, as shown in Figs. 3(a)–3(d). However, the topological network is absent in region I. Such a result demonstrated explicitly that region I (II) of the 1.15º TGB is in the unreconstructed (reconstructed) structure.

Since both the reconstructed and unreconstructed structures can be stable in TBG around the magic angle, therefore, it is reasonable to ask whether the two structures can be switchable. Previously, it has been demonstrated that the STM tip can reshape the topography of underneath graphene via the electrostatic force and/or van der Waals

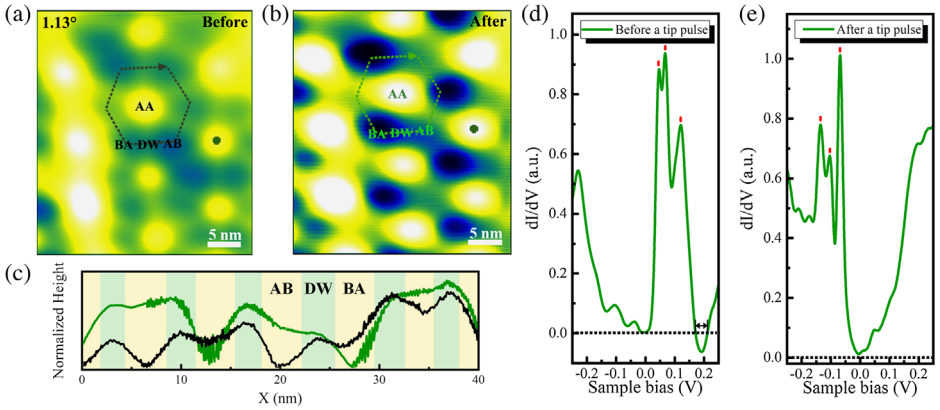

FIG. 4. (a) STM image ($V_S = 650$ mV and $I = 0.3$ nA) of a 1.13° TBG showing the reconstructed structure. (b) STM image of the same region as (a) after applying a 3-V tip pulse for 0.1 s. (c) Height profiles along dashed lines around the *AA* region in (a) and (b). The DW and *AB* and *BA* regions are marked with different colors. (d),(e) Typical STS spectra taken at the same position marked by solid dots in (a) and (b).

force [50–58]. Here, we demonstrated that the two structures in TBG near the magic angle can be switched to each other by applying a STM tip pulse. Figure 4 summarizes the result obtained in a 1.13° TBG. Before applying a STM tip pulse, the 1.13° TBG is in the reconstructed structure and exhibits sharp DWs linking different *AA* regions in the STM image, as shown in Fig. 4(a). After applying a 3-V tip pulse for 0.1 s, the morphology of the TBG changes a lot under the same imaging bias. The sharp DW network almost vanishes, and the size of the *AA* stacking region enlarges, as shown in Fig. 4(b) (see Supplemental Fig. S7 for FFT images of the two cases [26]). Figure 4(c) shows the height profiles along the dashed arrows in Figs. 4(a) and 4(b). Six well-defined corrugated DWs can be detected around each *AA* region before applying the tip voltage, and they become less visible after the pulse. For the extra structures connecting the *AA* domains [Fig. 4(b)], it is mainly caused by the strain in the TBG. Here the electrostatic force may play a dominant role because of the short time and large value of the tip voltage. This sudden applied energy perturbation leads to a structural transition of the TBG. In our experiment, we also find that the structure of the TGB can be tuned back to its original state by the tip pulse (see Supplemental Fig. S8 [26]). Therefore, our experiment demonstrated explicitly that the triangular network of chiral one-dimensional states hosted by domain boundaries can be switched on and off in TBG around the magic angle. The STM tip can locally reshape the topography of TBG via a pulse of tunneling voltage, which overcomes the energy barrier between the bistable structures.

The change of lattice reconstruction in the 1.13° TBG strongly alters its low-energy flat bands, as shown by the STS spectra in Figs. 4(d) and 4(e). The spectra recorded in the *AA* regions show low-energy sharp peaks, which correspond to the flat bands of TBG [41,42,46–48,59]. We can make three observations from the spectra. First, the doping of the TBG is changed: The flat bands are changed from fully empty [Fig. 4(d)] to fully occupied [Fig. 4(e)], which may partially arise from the variation of charge transfer between the TBG and the substrate because of the stimulus bias of the STM tip. Additionally, the enhanced next-nearest-neighbor hopping in strained TBG also can change the electron doping [41]. Second, the total full width at half maximum (FWHM) of the three subpeaks in the reconstructed TBG [Fig. 4(d)], ~105 meV, is larger than that in the unreconstructed TBG [Fig. 4(e)], ~70 meV. The third feature is the appearance of negative differential conductance between the flat bands and the high-energy conduction bands in the spectrum recorded in the reconstructed TBG [Fig. 4(d)], which is a clear signature that there is a gap between the flat bands and the high-energy conduction bands [60,61] (see Supplemental Fig. S9 for data of another sample [26]). To further understand the observed phenomena, we calculated the band structure and DOS of the MATBG with and without lattice relaxation (see Supplemental Fig. S10 for details [26]). The essential features of the broadened and isolated flat bands in the reconstructed TBG can be reproduced by our theoretical calculation. However, the extra splitting [three subpeaks in Figs. 4(d) and 4(e)] of the flat bands may be induced by the strain effects in the TGB, which is not involved in the calculation, according to previous studies [61,62]. Very recently, it was demonstrated explicitly that the heterostrain can efficiently reconstruct the band structure and lead to three resonant peaks in TBG around the magic angle [62,63]. Therefore, our experiment demonstrated explicitly that the lattice reconstruction in TBG around the magic angle can be manipulated locally via STM tip pulses, which, consequently, can switch on and off the DW network and tune the low-energy flat bands. Because the electronic correlation in MATBG depends on the

bandwidth of the flat bands [8–13,46–48,59], therefore, our result provides a new route to manipulate the correlated electronic phases.

Similar measurement, i.e., by applying a pulse of tunneling voltage, has been carried out in TBG with a twist angle that is much larger (or smaller) than the magic angle in our experiment (see Supplemental Figs. S11 and S12 [26]). However, structures of TBG below and above the magic angle are quite stable and almost unchanged by the tip pulse.

In summary, we demonstrated that both the reconstructed and unreconstructed structures are stable in TBG around the magic angle and they can be switched to each other. This provides a method to manipulate the electronic property of magic angle TBG through tunable lattice reconstruction, which can also be extended to transition metal dichalcogenide twisted bilayers [64].

This work was supported by the National Natural Science Foundation of China (Grants No. 11974050 and No. 11674029). L. H. also acknowledges support from the National Program for Support of Top-notch Young Professionals, support from "the Fundamental Research Funds for the Central Universities," and support from "Chang Jiang Scholars Program." Y. S. was supported by the U.S. Department of Energy through the Los Alamos National Laboratory (LANL) LDRD program and was supported by the Center for Non-linear Studies at LANL.

*Corresponding author.
helin@bnu.edu.cn
†These authors contributed equally to this work.

[1] J. M. B. Lopes dos Santos, N. M. R. Peres, and A. H. Castro Neto, Phys. Rev. Lett. **99**, 256802 (2007).
[2] G. Li, A. Luican, J. M. B. Lopes dos Santos, A. H. Castro Neto, A. Reina, J. Kong, and E. Y. Andrei, Nat. Phys. **6**, 109 (2010).
[3] A. Luican, G. Li, A. Reina, J. Kong, R. R. Nair, K. S. Novoselov, A. K. Geim, and E. Y. Andrei, Phys. Rev. Lett. **106**, 126802 (2011).
[4] I. Brihuega, P. Mallet, H. González-Herrero, G. Trambly de Laissardière, M. Ugeda, L. Magaud, J. M. Gómez-Rodríguez, F. Ynduráin, and J.-Y. Veuillen, Phys. Rev. Lett. **109**, 196802 (2012).
[5] W. Yan, M. Liu, R.-F. Dou, L. Meng, L. Feng, Z.-D. Chu, Y. Zhang, Z. Liu, J.-C. Nie, and L. He, Phys. Rev. Lett. **109**, 126801 (2012).
[6] T. Ohta, J. T. Robinson, P. J. Feibelman, A. Bostwick, E. Rotenberg, and T. E. Beechem, Phys. Rev. Lett. **109**, 186807 (2012).
[7] R. Bistritzer and A. H. MacDonald, Proc. Natl. Acad. Sci. U.S.A. **108**, 12233 (2011).
[8] Y. Cao, V. Fatemi, A. Demir, S. Fang, S. L. Tomarken, J. Y. Luo, J. D. Sanchez Yamagishi, K. Watanabe, T. Taniguchi, E. Kaxiras, R. C. Ashoori, and P. Jarillo-Herrero, Nature (London) **556**, 80 (2018).
[9] Y. Cao, V. Fatemi, S. Fang, K. Watanabe, T. Taniguchi, E. Kaxiras, and P. Jarillo-Herrero, Nature (London) **556**, 43 (2018).
[10] X. Lu, P. Stepanov, W. Yang, M. Xie, M. A. Aamir, I. Das, C. Urgell, K. Watanabe, T. Taniguchi, G. Zhang, A. Bachtold, A. H. MacDonald, and D. K. Efetov, Nature (London) **574**, 653 (2019).
[11] M. Yankowitz, S. Chen, H. Polshyn, Y. Zhang, K. Watanabe, T. Taniguchi, D. Graf, A. F. Young, and C. R. Dean, Science **363**, 1059 (2019).
[12] A. L. Sharpe, E. J. Fox, A. W. Barnard, J. Finney, K. Watanabe, T. Taniguchi, M. A. Kastner, and D. Goldhaber-Gordon, Science **365**, 605 (2019).
[13] M. Serlin, C. L. Tschirhart, H. Polshyn, Y. Zhang, J. Zhu, K. Watanabe, T. Taniguchi, L. Balents, and A. F. Young, Science **367**, 900 (2020).
[14] M. M. van Wijk, A. Schuring, M. I. Katsnelson, and A. Fasolino, 2D Mater. **2**, 034010 (2015).
[15] F. Gargiulo and O. V. Yazyev, 2D Mater. **5**, 015019 (2017).
[16] K. Zhang and E. B. Tadmor, J. Mech. Phys. Solids **112**, 225 (2018).
[17] N. R. Walet and F. Guinea, 2D Mater. **7**, 015023 (2019).
[18] N. N. T. Nam and M. Koshino, Phys. Rev. B **96**, 075311 (2017).
[19] H. Yoo, R. Engelke, S. Carr, S. Fang, K. Zhang, P. Cazeaux, S. H. Sung, R. Hovden, A. W. Tsen, T. Taniguchi, K. Watanabe, G.-C. Yi, M. Kim, M. Luskin, E. B. Tadmor, E. Kaxiras, and P. Kim, Nat. Mater. **18**, 448 (2019).
[20] S. Carr, S. Fang, Z. Zhu, and E. Kaxiras, Phys. Rev. Research **1**, 013001 (2019).
[21] S. Fang, S. Carr, Z. Zhu, D. Massatt, and E. Kaxiras, arXiv:1908.00058 (2019).
[22] S. Jin *et al.*, Science **362**, 1021 (2018).
[23] Z. Zhang, X. Xu, Z. Zhang, M. Wu, J. Wang, C. Liu, N. Shang, J. Wang, P. Gao, D. Yu, E. Wang, and K. Liu, Adv. Mater. Interfaces **5**, 1800377 (2018).
[24] K. Kim, S. Coh, L. Z. Tan, W. Regan, J. M. Yuk, E. Chatterjee, M. F. Crommie, M. L. Cohen, S. G. Louie, and A. Zettl, Phys. Rev. Lett. **108**, 246103 (2012).
[25] X. Xu *et al.*, Sci. Bull. **62**, 1074 (2017).
[26] See Supplemental Material at http://link.aps.org/supplemental/10.1103/PhysRevLett.125.236102 for more experimental data, analysis, details of calculations, and discussion, which includes Refs. [27–32].
[27] C. R. Woods, L. Britnell, A. Eckmann, G. L. Yu, R. V. Gorbachev, A. Kretinin, J. Park, L. A. Ponomarenko, M. I. Katsnelson, Y. N. Gornostyrev, K. Watanabe, T. Taniguchi, C. Casiraghi, A. K. Geim, and K. S. Novoselov, Nat. Phys. **10**, 451 (2017).
[28] H. Shi, Z. Zhan, Z. Qi, K. Huang, E. van Veen, J. A. Silva-Guillen, R. Zhang, P. Li, K. Xie, H. Ji, M. I. Katsnelson, S. Yuan, S. Qin, and Z. Zhang, Nat. Commun. **11**, 371 (2020).
[29] J. Mao, S. P. Milovanovic, M. Andelkovic, X. Lai, Y. Cao, K. Watanabe, T. Taniguchi, L. Covaci, F. M. Peeters, A. K. Geim, Y. Jiang, and E. Y. Andrei, Nature (London) **584**, 215 (2020).
[30] Nguyen N. T. Nam and Mikito Koshino, Phys. Rev. B **96**, 075311 (2017).
[31] H. Suzuura and T. Ando, Phys. Rev. B **65**, 235412 (2002).

[32] J. L. Mañes, Phys. Rev. B **76**, 045430 (2007).
[33] F. Guinea, M. I. Katsnelson, and M. A. H. Vozmediano, Phys. Rev. B **77**, 075422 (2008).
[34] L.-J. Yin, H. Jiang, J.-B. Qiao, and L. He, Nat. Commun. **7**, 11760 (2016).
[35] I. Martin, Y. M. Blanter, and A. F. Morpurgo, Phys. Rev. Lett. **100**, 036804 (2008).
[36] F. Zhang, A. H. MacDonald, and E. J. Mele, Proc. Natl. Acad. Sci. U.S.A. **110**, 10546 (2013).
[37] A. Vaezi, Y. Liang, D. H. Ngai, L. Yang, and E.-A. Kim, Phys. Rev. X **3**, 021018 (2013).
[38] P. San-Jose and E. Prada, Phys. Rev. B **88**, 121408(R) (2013).
[39] S. Dai, Y. Xiang, and D. J. Srolovitz, Nano Lett. **16**, 5923 (2016).
[40] S. Huang, K. Kim, D. K. Efimkin, T. Lovorn, T. Taniguchi, K. Watanabe, A. H. MacDonald, E. Tutuc, and B. J. LeRoy, Phys. Rev. Lett. **121**, 037702 (2018).
[41] J. B. Qiao, L. J. Yin, and L. He, Phys. Rev. B **98**, 235402 (2018).
[42] L.-J. Yin, J.-B. Qiao, W.-J. Zuo, W.-T. Li, and L. He, Phys. Rev. B **92**, 081406(R) (2015).
[43] S.-Y. Li, K.-Q. Liu, L. J. Yin, W. X. Wang, W. Yan, X. Q. Yang, J. K. Yang, H. Liu, H. Jiang, and L. He, Phys. Rev. B **96**, 155416 (2017).
[44] W.-J. Zuo, J.-B. Qiao, D.-L. Ma, L.-J. Yin, G. Sun, J.-Y. Zhang, L.-Y. Guan, and L. He, Phys. Rev. B **97**, 035440 (2018).
[45] W.-X. Wang, H. Jiang, Y. Zhang, S.-Y. Li, H. W. Liu, X. Li, X. Wu, and L. He, Phys. Rev. B **96**, 115434 (2017).
[46] Y. Jiang, J. Mao, X. Lai, K. Watanabe, T. Taniguchi, K. Haule, and E. Y. Andrei, Nature (London) **573**, 91 (2019).
[47] A. Kerelsky, L. McGilly, D. M. Kennes, L. Xian, M. Yankowitz, S. Chen, K. Watanabe, T. Taniguchi, J. Hone, C. Dean, A. Rubio, and A. N. Pasupathy, Nature (London) **572**, 95 (2019).
[48] Y. Choi, J. Kemmer, Y. Peng, A. Thomson, H. Arora, R. Polski, Y. Zhang, H. Ren, J. Alicea, G. Refael, F. von Oppen, K. Watanabe, T. Taniguchi, and S. Nadj-Perge, Nat. Phys. **15**, 1174 (2019).
[49] M. Fleischmann, R. Gupta, F. Wullschläger, S. Theil, D. Weckbecker, V. Meded, S. Sharma, B. Meyer, and S. Shallcross, Nano Lett. **20**, 971 (2020).
[50] N. N. Klimov, S. Jung, S. Zhu, T. Li, C. A. Wright, S. D. Solares, D. B. Newell, N. B. Zhitenev, and J. A. Stroscio, Science **336**, 1557 (2012).
[51] S.-Y. Li, K.-K. Bai, W.-J. Zuo, Y.-W. Liu, Z.-Q. Fu, W.-X. Wang, Y. Zhang, L.-J. Yin, J.-B. Qiao, and L. He, Phys. Rev. Applied **9**, 054031 (2018).
[52] Y. Zhang, Q. Yang, Y. N. Ren, and L. He, Phys. Rev. B **100**, 075435 (2019).
[53] S.-Y. Li, Y. Su, Y.-N. Ren, and L. He, Phys. Rev. Lett. **124**, 106802 (2020).
[54] M. Yankowitz, K. Watanabe, T. Taniguchi, P. San-Jose, and B. J. LeRoy, Nat. Commun. **7**, 13168 (2016).
[55] T. Mashoff, M. Pratzer, V. Geringer, T. J. Echtermeyer, M. C. Lemme, M. Liebmann, and M. Morgenstern, Nano Lett. **10**, 461 (2010).
[56] H. Baek, J. Ha, D. Zhang, B. Natarajan, J. P. Winterstein, R. Sharma, R. Hu, K. Wang, S. Ziemak, J. Paglione, Y. Kuk, N. B. Zhitenev, and J. A. Stroscio, Phys. Rev. B **92**, 094510 (2015).
[57] D. Wong, J. Velasco, Jr., L. Ju, J. Lee, S. Kahn, H. Z. Tsai, C. Germany, T. Taniguchi, K. Watanabe, A. Zettl, and F. Wang, Nat. Nanotechnol. **10**, 949 (2015).
[58] P. Jia, W. Chen, J. Qiao, M. Zhang, X. Zheng, Z. Xue, R. Liang, C. Tian, L. He, Z. Di, and X. Wang, Nat. Commun. **10**, 3127 (2019).
[59] Y. Xie, B. Lian, B. Jäck, X. Liu, C.-L. Chiu, K. Watanabe, T. Taniguchi, B. A. Bernevig, and A. Yazdani, Nature (London) **572**, 101 (2019).
[60] S. Y. Li, H. Liu, J. B. Qiao, H. Jiang, and L. He, Phys. Rev. B **97**, 115442 (2018).
[61] S.-Y. Li, Y. Zhang, Y.-N. Ren, J.-P. Liu, X. Dai, and L. He, Phys. Rev. B **102**, 121406(R) (2020).
[62] L. Huder, A. Artaud, T. Le Quang, G. T. de Laissardière, A. G. M. Jansen, G. Lapertot, C. Chapelier, and V. T. Renard, Phys. Rev. Lett. **120**, 156405 (2018).
[63] Y. Zhang, Z. Hou, Y.-X. Zhao, Z.-H. Guo, Y.-W. Liu, S.-Y. Li, Y.-N. Ren, Q.-F. Sun, and L. He, Phys. Rev. B **102**, 081403(R) (2020).
[64] A. Weston, Y. Zou, V. Enaldiev, A. Summerfield, N. Clark, V. Z'olyomi, A. Graham, C. Yelgel, S. Magorrian, M. Zhou, J. Zultak, D. Hopkinson, A. Barinov, T. Bointon, A. Kretinin, N. R. Wilson, P. H. Beton, V. I. Fal'ko, S. J. Haigh, and R. Gorbachev, Nat. Nanotechnol. **15**, 592 (2020).